

Article

Transparency of a Geographically Distributed Test Platform for Fuel Cell Electric Vehicle Powertrain Systems Based on X-in-the-Loop Approach

Wenxu Niu ¹, Ke Song ^{1,2,*}, Qiwen Xiao ³ , Matthias Behrendt ³, Albert Albers ³ and Tong Zhang ¹

¹ School of Automotive Studies, Tongji University, Shanghai 201804, China; jingjingjing2008@outlook.com (W.N.); tzhang@tongji.edu.cn (T.Z.)

² National Fuel Cell Vehicle and Powertrain System Engineering Research Center, Tongji University, Shanghai 201804, China

³ Institute of Product Engineering (IPEK), Karlsruhe Institute of Technology (KIT), 76131 Karlsruhe, Germany; qiwen.xiao@partner.kit.edu (Q.X.); matthias.behrendt@kit.edu (M.B.); albert.albers@kit.edu (A.A.)

* Correspondence: ke_song@tongji.edu.cn

Received: 15 August 2018; Accepted: 7 September 2018; Published: 12 September 2018



Abstract: X-in-the-loop is a new vehicle development and validation method for increasingly complex vehicle systems, which integrates the driver and the environment. In view of recent developments in fuel cell electric vehicle powertrain systems, Tongji University and Karlsruhe Institute of Technology have jointly developed a set of distributed test platforms based on the X-in-the-loop approach. This platform contains models and test equipment for a fuel cell electric vehicle powertrain system. Due to the involvement of remote connection and the Internet, test with connected test benches will suffer great uncertainty cause of signal transfer delay. To figure out this uncertainty, the concept of transparency is introduced. Four parameters were selected as transparency parameters in this distributed test platform. These include vehicle speed, fuel cell output power, battery output power, and electric motor torque under several different configuration settings. With the help of transparency theory and statistical methodology, especially Analysis of Variance (ANOVA), the transparency of these four parameters was established, vehicle speed, electric motor torque, battery power, and fuel cell power are affected by network state, the degree of influence is enhanced in turn. Using new defined parametric and non-parametric methods, this paper identifies the statistical significance and the transparency limitations caused by Internet under these several configurations. These methods will generate inputs for developer setting the distributed test configuration. These results will contribute to optimize the process of geographically distributed validation and joint development.

Keywords: X-in-the-loop; fuel cell electric vehicle; powertrain system; distributed test platform; transparency; nonparametric detection

1. Introduction

With the development of the automobile industry, the complexity of automobiles is increasing. Therefore, the development of vehicles is no longer a concern of individual companies, but has become a primary focus requiring the combined efforts of a number of companies. This is especially true in the case of electric vehicles, which require additional interdisciplinary cooperation from companies that have never dealt with the automotive industry before. Nowadays, collaboration in vehicle development can take place not only between developers in different locations, but also across companies. This multi-site product development is being studied at some research institutes as an important research field. The trend of globalization, the increasing complexity of automotive

products, the rapid change in technologies [1,2] as well as the regionalization of technical expertise [2], have presented new challenges for the automotive industry. Cooperative testing and validating tests between multiple regions or countries has now become a usual practice in industry. One way of realizing such a cooperation is to connect the globally distributed testing and validation parts through the Internet, which assures agreement on what parts to assemble when distributed parts are brought together for local tests [3]. Further advantages of this method include a guarantee that participants will share confidential information eliminates inclusion of those who are unwilling to share their knowledge or prototypes with partners who realize the importance of IP cooperation.

Aimed at simplifying the increasingly complex vehicle system, X-in-the-loop development and validation theory has been led by Professor Albers at the Karlsruhe Institute of Technology. He and other scholars have integrated simulation models and real components, making full use of existing tools and methods to assess the impacts of drivers and the external environment on electric vehicle requirements and development processes [3–5]. The core benefit of the theory is its ability to enable continuance when a test component is missing through models or code, which can replace the missing parts [6,7]. In this way, hardware and software integration tests were successful [8–10]. By breaking through the limitation of physical connection, the concept of “X-in-the-loop” has been extended to “X-in-the-distance-loop”, which provides an innovative and inspirational way of testing and validating in the vehicle development process, creating more possibilities for the future of the electric vehicle and other advanced vehicles in the automotive industry [3,4].

However, despite the advances, questions remain unanswered, including: how to evaluate the effectiveness of the X-in-the distance loop’s development and validation theory, how to determine the difference between remote testing and local testing, and how to measure this difference. Remote development and validation with X-in-the-loop are used in other applications such as space manipulator remote operation and remote surgery, with comparative procedures. Evaluating indicators in these areas can be used as references as similarities surface between these technologies and the new remote automotive technology. In the field of space manipulator remote operation, the concept “transparency” refers to accuracy of the force and displacement between the robot slave arm and the main arm, which allows the operator to offer input based on his or her subjective, intellectual and experienced connectivity to the direct operation of the environment [11]. Combining the practical problems of teleoperation manipulators and space exploration, Lawrence et al. [12,13] put forward a measure of transparency, which measures the subjective feelings of remote distributed system operators. Thus, system transparency will be ideal when transmission impedance and environmental impedance are equal. In addition, Natori et al. [14,15] used the correspondence between the position and the force signal, which is named **H** matrix, to measure the transparency.

It is worth noting that the above methods are aimed at linear systems, which are for parameters of a set value. In a distributed nonlinear system, the coupling relationship is complicated; thus, it is hard to calculate impedance or **H** matrix, which makes a transparency description method for non-linear systems necessary. Since in the linear system, force and position are measures of subjective feelings, in a nonlinear system, it is necessary to look for quantitative relationships between variables and subjective feelings. In the field of psychology, the Weber-Fechner law shows the relationship between psychological and physical quantities, that is, the difference between the threshold of a change with an amount of stimulation changes, while still showing a certain regularity. Φ is the original amount of stimulation, $\Delta\Phi$ is the difference in threshold at this time, and C is the ratio of $\Delta\Phi$ and Φ , also known as Weber rate [16]. The Weber-Fechner Law has been introduced into the field of robot tactile perception, and the Friedman statistical method is used to measure the comprehensive performance of the robot arm [17]. Here quantitative relationships between variables and subjective feelings are established.

Furthermore, the Analysis of Variance (ANOVA) method is used to measure and compare the transparency of the system [18]. Assuming the existence of n different types of experimental conditions (here, this specifically refers to different structural conditions), in each type of experimental condition, the experiments repeat m times. According to the mean value of the standard deviation, p -value was

carried out by using the analysis of variance method. Furthermore, the robustness and transparency were discussed according to the p -value. Here levels of p -value represent whether the transparency of objects to be compared is consistent.

In this paper, the distributed test platform is located in China and Germany with Internet data exchange interaction. Because Internet data transmission has the characteristics of uncertain delay and packet loss, additional uncertainty is added to the system [19,20]. Whether the additional uncertainty can be ignored should be discussed. To find out the differences between remote operation and local operation, four transparency parameters were selected, including vehicle speed, fuel cell output power, battery output power and electric motor torque under several different configuration settings in this distributed test platform. With the help of the transparency theory and statistical method, transparency comparisons of these four parameters were carried out. Using parametric and non-parametric detection, the statistical significance and transparency limitations caused by the Internet under these configurations were determined.

2. System Model

2.1. Structure of Distributed Test Platform

Tongji University in Shanghai, China and Karlsruhe Institute of Technology (KIT) in Karlsruhe, Germany jointly developed a distributed test platform for a fuel cell electric vehicle powertrain system based on X-in-the-loop approach. This platform aimed at calculating the energy consumption of the fuel cell drivetrain system and validating the fuel economy of the fuel cell vehicle drivetrain system. Another goal was to remotely connect the distributed platform's developed environment and data transfer capability between two computers—one in China at Tongji University and the other in Germany at KIT. In KIT, we used a MiniHiL as a vehicle axle to connect the road and transmission and to create a model running at real-time machine rates to integrate the E-motor and transmission. The next task was to include the driver model and energy resource model with a fuel cell and battery, which were placed in a real-time machine in Tongji. Since we tried to compare the results from different connection settings, these two parts were placed on both sides of the virtual or physical model as a configuration requirement. The whole structure of this distributed test platform is shown in Figure 1.

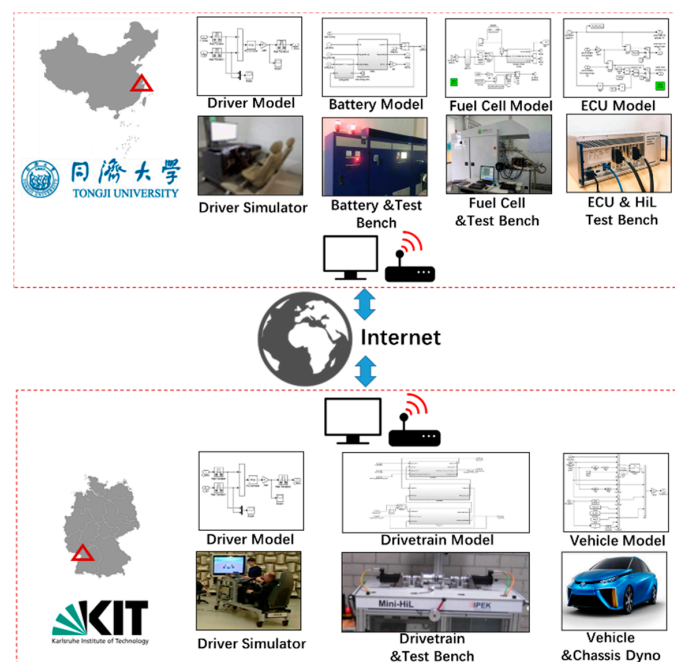


Figure 1. Structure of distributed test platform for fuel cell electric vehicle powertrain system.

According to test targets, the virtual models or hardware on both sides can be combined flexibly. Aimed at transparency research, on the Chinese side of the driver model, the electric control unit (ECU) model, battery model and fuel cell model were chosen, while on German side, the drivetrain model, drivetrain hardware (MiniHiL test bench) and vehicle model were chosen. The data flow between both sides and models are shown in Figure 2.

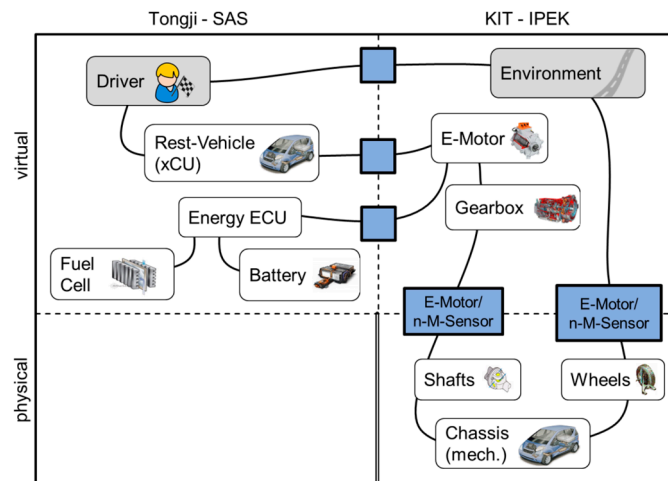


Figure 2. Data flow of distributed test platform aimed at transparency research.

2.2. Model of Objects

2.2.1. Powertrain Configuration of Demo Fuel Cell Electric Vehicle

This article focuses on a vehicle’s powertrain system shown in Figure 3. The power sources consist of a fuel cell range extender and a battery system for the sake of quick dynamic response and durability. The fuel cell system can drive the motors and simultaneously charge the battery [21].

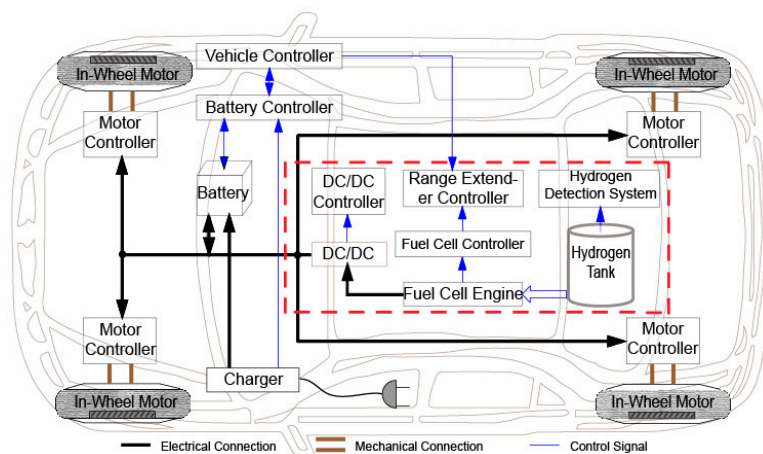


Figure 3. Structure of fuel cell electric vehicle powertrain system.

2.2.2. The Longitudinal Dynamic Model of Vehicle

In order to simulate actual velocity and complete remote driver simulation, it is necessary to build a longitudinal dynamic model of the electric vehicle. The longitudinal dynamic equation of the vehicle is shown in Equation (6) [22]:

$$\frac{T_{tq} i_g \eta_T}{r_t} = m_v g f_R + \frac{1}{2} C_w A \rho_a \dot{x}^2 + \delta m \ddot{x} \tag{1}$$

The vehicle parameters are listed in Table 1 [23].

Table 1. Vehicle parameters.

Name	Parameter	Unit	Symbol
Vehicle weight	1600	kg	m_v
Transmission ratio	1	-	i_g
Transmission system efficiency	92	%	η_T
Tire radius	0.3	m	r_t
Rolling resistance coefficient	0.01	-	f_R
Air resistance coefficient	0.35	-	C_w
Frontal area	2.8	m ²	A
10 °C sea level air density	1.2	N·s ² ·m ⁻⁴	ρ_a
Rotational mass conversion factor	1.05	-	δ
Drive torque	-	N·m	T_{tq}
Vertical speed	-	m/s	\dot{x}
Vertical acceleration	-	m/s ²	\ddot{x}

According to the longitudinal dynamic equation, vehicle can be obtained based on drive torque.

2.2.3. Fuel Cell Model

Proton exchange membrane fuel cells (PEMFC) use hydrogen and oxygen as fuels to generate electrical energy through electrochemical reactions. The oxidation reaction of the anode and the reduction reaction of the cathode are shown in the following formulas [24]:



The fuel cell covers theoretical knowledge including material science, fluid mechanics, thermodynamics and electrochemistry, and its working mechanism can hardly be described by a clear mathematical relation. The complexity of the fuel cell subsystem also makes the dynamic response of fuel cells worse and more affected by their surrounding working environment. At present, a simplified model is established with reference to the models of [25,26]. In order to describe a fuel cell system more accurately, parameter identification and data fitting are common methods to improve the accuracy of the simplified model and to make its applicability easier to understand. When the load current changes, due to the charging effect, the fuel cell's bipolar plate surface produces a slowly changing voltage. The equivalent resistance R_a is connected in parallel with a capacitor C , as shown in the specific equivalent model diagram of Figure 4.

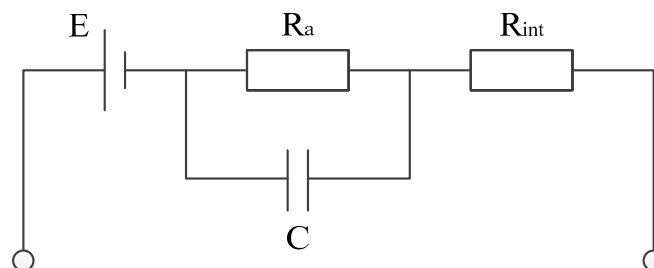


Figure 4. Fuel cell equivalent circuit model diagram.

The relationship between the fuel cell internal variables is shown as follows:

$$U_{R_a} = U_C = I \cdot R_a \times \left(1 - e^{-\frac{I}{R_a C}}\right) \quad (5)$$

$$U_m = E - I \cdot R_{int} - I \cdot R_a \times \left(1 - e^{-\frac{I}{R_a C}}\right) \quad (6)$$

$$U_{stack} = U_m \cdot n \quad (7)$$

$$P_{fc_out} = U_{stack} \times I = n \times \left[EI - I^2 R_{int} - I^2 R_a \left(1 - e^{-\frac{I}{R_a C}}\right) \right] \quad (8)$$

The fuel cell symbols are shown in Table 2.

Table 2. Fuel cell symbols.

Name	Symbol
equivalent resistance	R_a
equivalent capacitor	C
output current	I
R_a voltage	U_{R_a}
C voltage	U_c
fuel cell single voltage	U_m
electromotive force of single cell	E
internal resistance	R_{int}
fuel cell output voltage	U_{stack}
number of single cell	n
output power of the fuel cell	P_{fc_out}

The output power-efficiency curve of fuel cell is shown in Figure 5. Other fuel cell values are shown in Table 3.

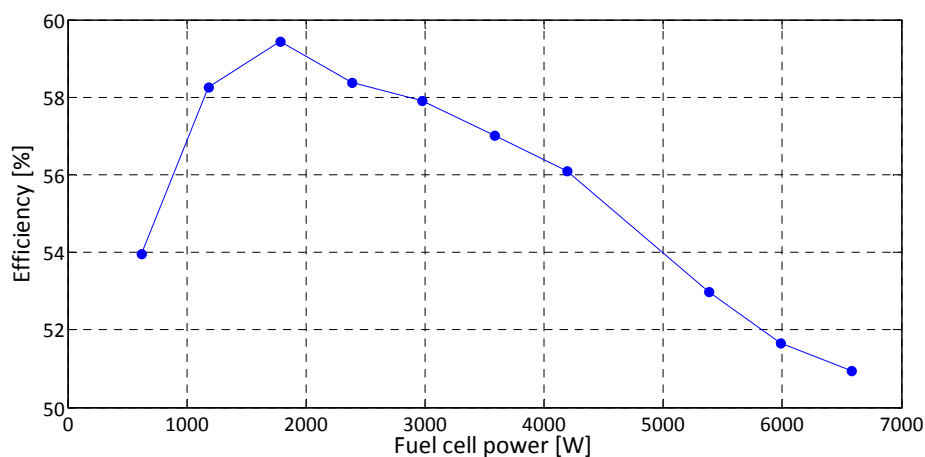


Figure 5. Output power-efficiency curve of fuel cell.

Table 3. Fuel cell values.

Name	Value	Unit
Single fuel cell internal resistance	0.0003	Ω
Single fuel cell equivalent resistance	0.0006	Ω
Single fuel cell open circuit voltage	1.037	V
Single fuel cell equivalent capacitor	3	F
Fuel cell rated power	6	kW
Fuel cell peak power	6.5	kW

2.2.4. Battery

The battery can make up for the lack of dynamic response of the fuel cell and absorb the energy of the brake [27–29]. Here a packaged ternary polymer lithium battery model is used. Battery and fuel cell are connected in parallel, using a power following strategy. In this paper, the analytic model of the battery will be used. The input is battery current and temperature, and the output will be voltage and State of Charge (SOC). By stationary state the charging mode of our vehicle is constant current-constant voltage (CC-CV) cycle. For this battery model, the following assumptions exist: the internal resistance of the battery model is constant, that is, the internal resistance value is kept constant during the charging and discharging process of the battery, and is also independent of the charge and discharge current; there is no memory effect in the battery. The battery model is mainly divided into three modules: SOC calculation module, voltage calculation module, and a thermal calculation module. The input and output of the battery model and energy management strategy can be expressed as:

$$SOC = \frac{Q_c - \int idt}{Q_c} \times 100\% \quad (9)$$

$$U_b = \left(OCV(SOC) - U_{drop}(i)\right) \cdot N_s \quad (10)$$

$$P_{b_in} = P_{in} - \eta \cdot P_{fc_out} \quad (11)$$

$$P_{out} = \eta \cdot P_{fc_out} + P_{b_out} \quad (12)$$

The battery symbols are shown in Table 4.

Table 4. Battery symbols.

Name	Symbol
capacity of battery cell	Q_c
battery cell current	i
cell open circuit voltage	OCV
voltage drop in battery cell	U_{drop}
battery output power	P_{b_out}
battery utilization efficiency function	f_P
battery demand power	P_{b_in}
battery voltage	U_b
system demand power	P_{in}
efficiency of fuel cell DC/DC	η
output power of fuel cell and battery	P_{out}

The maximum capacity of the battery is related to temperature. The cell open circuit voltage-SOC diagram is shown in Figure 6. Other battery values are shown in Table 5.

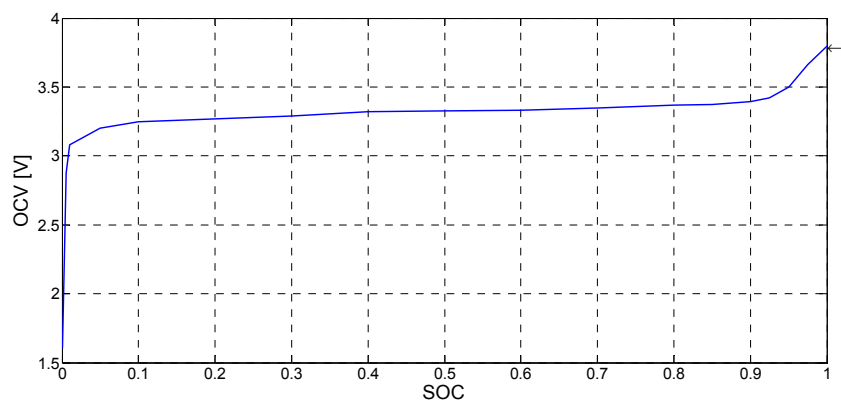


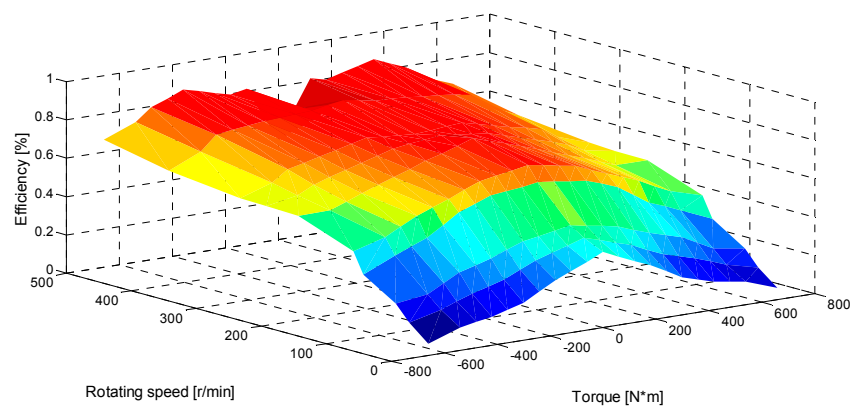
Figure 6. Power battery cell open circuit voltage-SOC curve.

Table 5. Battery values.

Name	Value	Unit
Maximum current	500	A
Maximum charge current	−45	A
Number of series batteries	100	-
Number of parallel batteries	20	-
Battery cell radius	0.013	m
Battery cell height	0.065	m
Battery cell capacity	2.3×3600	Ah·s
C-rate (charge-discharge current/rated capacity)	1	C

2.2.5. Electric Motor

The drivetrain contains four in-wheel electric motors. Here, the electric motor model is a quasi-steady-state model. The relationship between torque, rotating speed, and efficiency is shown in Figure 7. The electric motor values are shown in Table 6.

**Figure 7.** Relationship between torque, rotating speed, and efficiency.**Table 6.** Electric motor values.

Name	Value	Unit
Drive Type	4 In-Wheel Motor	-
In-Wheel Motor Rated/Peak Power	$4 \times 0.8/4 \times 2.5$	kW

2.2.6. Drivetrain Test Bench

Before the new test configurations are implemented on the high power test benches, they can first be tested on relatively lower power test benches. The goal is to create a development and test environment for new test configurations without compromising the operation on the test stands. For this purpose, a Mini Hardware-in-the-Loop test bench (MiniHiL), which is shown in Figure 8, was used to create a development environment for new test configurations. Notably, the Mini-HiL proved to be a particularly suitable test bench for this preliminary study.

Further considering the combination of hardware and software, corresponding to the drivetrain model, the MiniHiL test bench was used to replace the drivetrain model. The MiniHiL test bench consists of two electric motors with 1.5 kW power and 6000 min^{-1} peak speed, with a connecting shaft. Here, one motor can be used as a driving motor, and the other motor can be used as a loading motor. The electric motor parameters are shown in Table 7 [30].



Figure 8. MiniHiL test bench.

Table 7. Electric motor parameters.

Parameter	Value
Rated power	1.5 kW
Rated torque	2.4 Nm
Maximum rotating speed	6000 r/min
Rated rotating speed	2500 r/min
Maximum torque	10.3 Nm

2.3. Communication Settings

In order to ensure communication between the hardware and software for efficiency and long-distance communication quality between the two PCs, a User Datagram Protocol (UDP) was used with virtual private network (VPN) components to ensure the speed of communication and security. Between the MiniHiL platform and the PC on the KIT side, the Controller Area Network (CAN) communication protocol was used to meet the MiniHiL platform communication standards. In addition, considering the actual PCs, computing ability and storage capacity, all PCs used the Ode3 solver, and the simulation step was 0.001 s.

3. Configuration Settings

3.1. Configuration Settings on Location, Hardware and Software

Any difference in the whole structure configuration can have a potential impact on transparency; hence, it is important to set several different configurations, including different locations, hardware and software. A variable-control approach was used to measure the impact of different configurations. The configuration settings on location, hardware and software are shown in Table 8 and details are described afterwards. Because of some hardware factors of the physical object, this paper analyzes the network impact from the two settings of simulation and hardware test. Therefore, in the following table, the tests were divided into A1–A4, (simulation test), B1–B3 (physical test).

Table 8. Configuration settings on location, hardware and software.

Serial Number	Location	Roundtrip Delay	Operating Environment
Configuration A1	Same location	0	Simulation environment
Configuration A2	Same location	0.4s	Simulation environment
Configuration A3	Same location	Real time campus Ethernet delay	Simulation environment
Configuration A4	China and Germany	Real time Internet delay	Simulation environment
Configuration B1	Same location	0	Simulation environment with MiniHiL
Configuration B2	Same location	0.4s	Simulation environment with MiniHiL
Configuration B3	China and Germany	Real time Internet delay	Simulation environment with MiniHiL

3.1.1. Configuration A1

Configuration A1 is under the MATLAB/Simulink simulation environment, which ran a fuel cell powertrain system model, including a driver model, vehicle longitudinal dynamic model, fuel cell model, power battery model and an electric drive system model. All models ran on the same PC. The conditions were tested as per the worldwide harmonized light duty test cycle (WLTC). This configuration is a total simulation environment without hardware components. This configuration is simulation environment standard.

3.1.2. Configuration A2

Configuration A2 is a MATLAB/Simulink simulation environment, under WLTC operating conditions, running the fuel cell powertrain system model, including two modules—each with different models: Module I contains the driver model, the fuel cell model, and the battery model. Module II contains the vehicle longitudinal dynamic model and the electric drive system model as module II. Between the two modules, a one-way 0.2 s delay (roundtrip 0.4 s) is added. The significance of Configuration A2 is that the ideal state output of the fuel cell powertrain system under the fixed delay condition is given in the simulation environment.

3.1.3. Configuration A3

Based on the Configuration A2, Module I and Module II are set in two PCs. Both PCs are in Tongji University. The significance of Configuration A3 is that the output of the fuel cell powertrain system under an Ethernet delay condition is given in a simulation environment.

3.1.4. Configuration A4

Based on Configuration A3, PC1 and PC2 were placed in Tongji and KIT. With Configuration A4 the output of the various parts of the fuel cell powertrain system under long-distance conditions is given.

3.1.5. Configuration B1

Configuration B1 follows the set up in Configuration A2 except that the drivetrain model is replaced by a MiniHiL test bench. The MiniHiL test bench is shown in Figure 4. All the components are in the same place. The delay between two modules is set to 0. This configuration gives the output of each part of the fuel cell powertrain system under the condition of a real electric motor, and other parts are in the form of a simulated model.

3.1.6. Configuration B2

Configuration B2 has a similar setup to Configuration A3 and Configuration B1. The drivetrain model is replaced by the MiniHiL test bench. Other models of the operating environment remain unchanged. The one-way 0.2 s delay (roundtrip 0.4 s) between the two PCs is set.

3.1.7. Configuration B3

Under Configuration B3, the MiniHiL test bench is placed in KIT and the other components are in Tongji. Configuration B3 gives the output of each part of the fuel cell powertrain system under the condition of the Internet.

3.2. Responses under Different Configuration Settings

To analyze the responses under different configuration settings, the roundtrip time under different configuration settings is measured and shown in Figure 9 and Table 9.

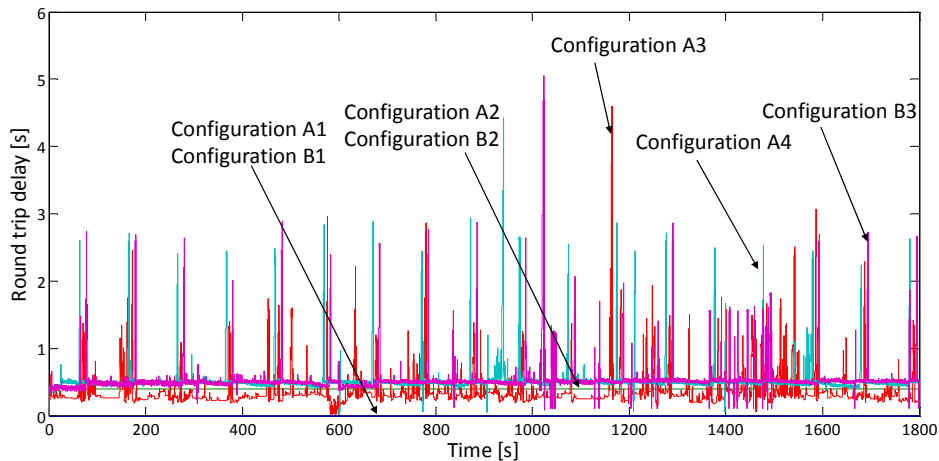


Figure 9. Roundtrip time under different configuration settings.

Table 9. Roundtrip delay parameters.

Configuration Type	Number of Packets	Min Delay	Max Delay	Average Delay	Standard Deviation
Configuration A1	180,001	0.0000	0.0000	0.0000	0.0000
Configuration A2	180,001	0.4000	0.4000	0.4000	0.0000
Configuration A3	180,001	0.0000	4.6000	0.3524	0.2630
Configuration A4	180,001	0.0000	4.4200	0.5205	0.2513
Configuration B1	180,001	0.0000	0.0000	0.0000	0.0000
Configuration B2	180,001	0.4000	0.4000	0.4000	0.0000
Configuration B3	180,001	0.0000	5.0400	0.5330	0.2571

As shown in Figure 9 and Table 9, the roundtrip delay of each configuration setting is different. It is worth noting that the hardware itself also has an impact on the round trip time. Under the condition that the delay of each configuration setting is different, the vehicle speed, fuel cell output power, battery output power, and the output torque of the electric motor are shown in Figures 10–13.

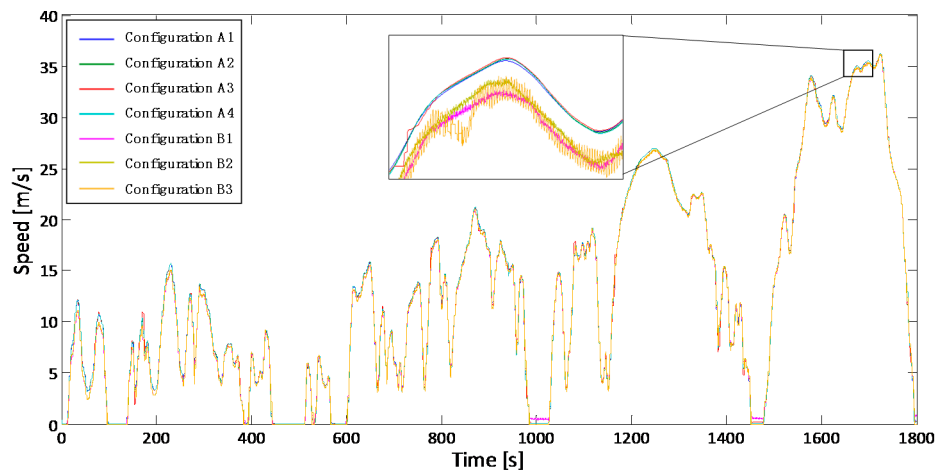


Figure 10. Speed response of fuel cell powertrain system under different configurations.

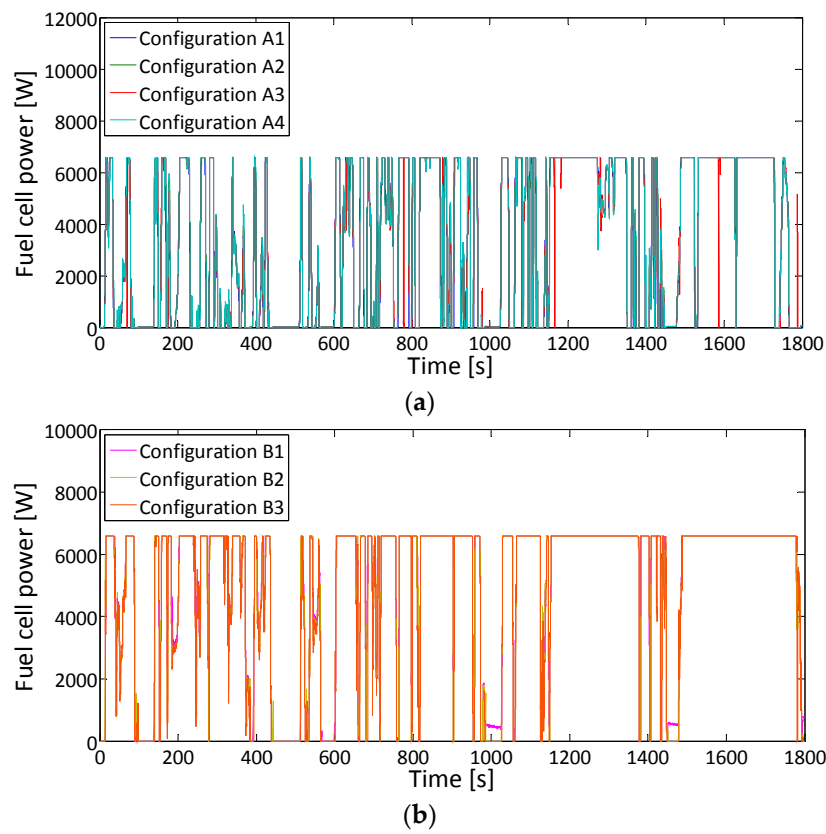


Figure 11. (a) Fuel cell output power under Configurations A1–A4; (b) Fuel cell output power under Configurations B1–B3.

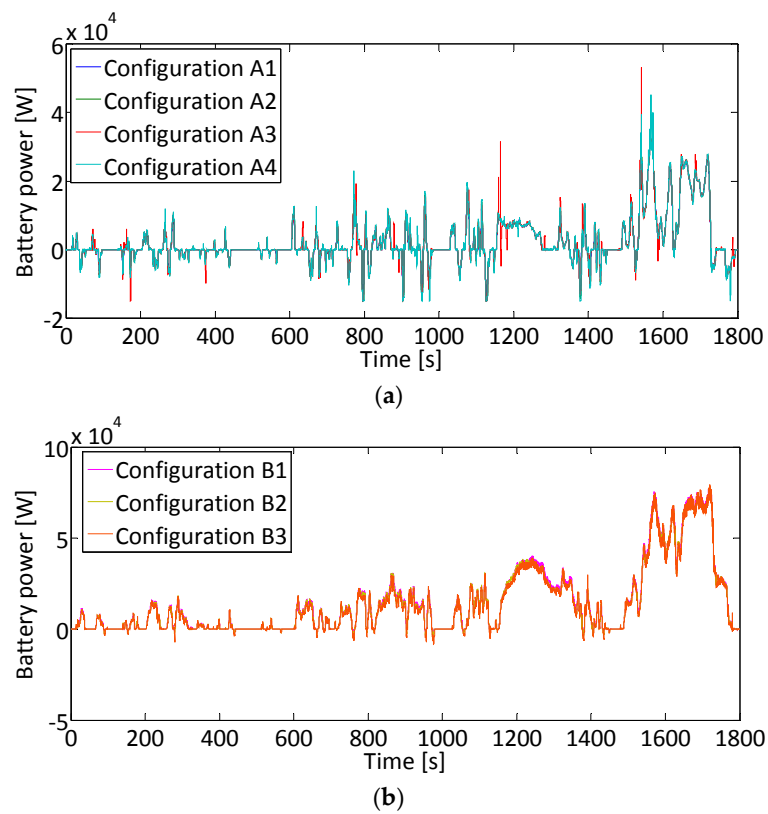


Figure 12. (a) Battery output power under Configurations A1–A4; (b) Battery output power under Configurations B1–B3.

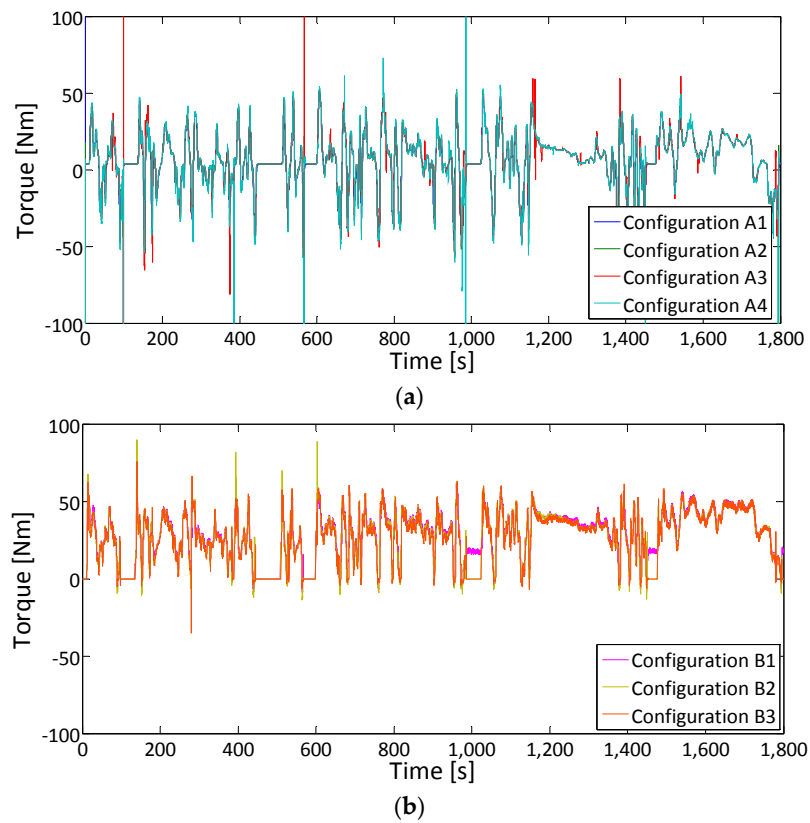


Figure 13. (a) Electric motor torque under Configurations A1–A4; (b) Electric motor torque under Configurations B1–B3.

While under Configuration A1–A4, all the components are in the form of a model. Under Configurations B1–B3, the Mini-HiL test bench is added, and the diagrams of fuel cell power, battery power and electric motor torque are divided into two parts.

4. Transparency Analysis

4.1. Nonparametric Statistical Analysis Method

From the above results, the system with several configurations is a nonlinear system. To evaluate the transparency of different configurations, a statistical analysis method, preferably the ANOVA method, should be considered. The ANOVA method was used in this research to measure the transparency of the system. With the ANOVA method, seven kinds of configurations can be regarded as seven different experimental conditions. In each type of experimental condition, the experiment is repeated three times. The standard deviation of the parameters is shown in the Tables 10–13. The data processing platform is IBM SPSS Statistics 19.

Table 10. The standard deviation of vehicle speed under different configurations (unit: m/s).

	Criterion: Configuration A1			Criterion: Configuration B1	
	Configuration A2	Configuration A3	Configuration A4	Configuration B2	Configuration B3
Test 1	0.0990	0.1633	0.1541	0.1798	0.8356
Test 2	0.0990	0.1970	0.1720	0.1870	0.1668
Test 3	0.0990	0.2236	0.1502	0.1726	0.1655
Average value	0.0990	0.1946	0.1588	0.1798	0.3893

Table 11. The standard deviation of fuel cell power under different configurations (unit: W).

	Criterion: Configuration A1			Criterion: Configuration B1	
	Configuration A2	Configuration A3	Configuration A4	Configuration B2	Configuration B3
Test 1	248.4924	566.8660	419.0964	365.9171	2686.9
Test 2	248.4924	488.0595	372.1072	293.0996	2644.1
Test 3	248.4924	456.3407	396.2455	587.1804	2653.3
Average value	248.4924	503.7554	395.8164	415.3990	2661.4

Table 12. The standard deviation of power battery power under different configurations (unit: W).

	Criterion: Configuration A1			Criterion: Configuration B1	
	Configuration A2	Configuration A3	Configuration A4	Configuration B2	Configuration B3
Test 1	547.2865	2164.2	830.0621	1102.7	3428.1
Test 2	547.2865	1044.4	930.7343	1278.9	1624.4
Test 3	547.2865	1184.2	861.0848	1121.2	1609.4
Average value	547.2865	1464.3	873.9604	1167.6	2200.6

Table 13. The standard deviation of electric motor torque under different configurations (unit: Nm).

	Criterion: Configuration A1			Criterion: Configuration B1	
	Configuration A2	Configuration A3	Configuration A4	Configuration B2	Configuration B3
Test 1	3.5937	4.3321	5.8564	4.5379	36.2328
Test 2	3.5937	4.1277	5.8548	4.2710	16.9457
Test 3	3.5937	4.3115	5.9193	4.7106	39.9875
Average value	3.5937	4.2571	5.8768	4.5065	31.0553

The variance homogeneity test is an important prerequisite for the ANOVA. The ANOVA method requires that the samples under the respective processing conditions come from the normal distribution respectively. Therefore, using the results of Tables 10–13 the variance homogeneity tests were carried out. Test results are shown in Tables 14–17.

Table 14. Variance homogeneity test result of vehicle speed.

Criterion	Levene	df1	df2	Significance
Configuration A1	0.936	3	720,000	0.422
Configuration B1	3.508	2	540,000	0.030

Table 15. Variance homogeneity test result of fuel cell output power.

Criterion	Levene	df1	df2	Significance
Configuration A1	6.973	3	720,000	0.000
Configuration B1	750.686	2	540,000	0.000

Table 16. Variance homogeneity test result of battery output power.

Criterion	Levene	df1	df2	Significance
Configuration A1	28.844	3	720,000	0.000
Configuration B1	120.278	2	540,000	0.000

Table 17. Variance homogeneity test result of electric motor output torque.

Criterion	Levene	df1	df2	Significance
Configuration A1	546.631	3	720,000	0.000
Configuration B1	542.999	2	540,000	0.000

As shown in Tables 14–17, except for vehicle speeds under Configurations A1–A4, vehicle speeds under Configuration B1–B3, fuel cell power, battery power and electric motor torque, variance is not homogeneous. Since the ANOVA method requires that the samples under each processing condition should come from the normal distribution population, the ANOVA method cannot be used directly. Non-parametric analysis, also known as the distribution of a free test, was used to mainly solve the overall distribution of the unknown statistical inference and can complete the lower level of measurement data inferred. Common nonparametric methods include the Mann-Whitney U test, Kolmogorov-Smirnov test, Kruskal-Wallis test, etc. Here, the Kruskal-Wallis test is used. The Kruskal-Wallis test is a nonparametric test method that determines whether or not the distribution on the p -value is the same by observing values from multiple independent population samples. Hence, we set the expectation and variance of rank sum T_i in Group i :

$$\mu_{T_i} = \frac{n_i(N+1)}{2} \quad (13)$$

$$\sigma_{T_i}^2 = \frac{n_i(N-n_i)(N+1)}{12} \quad (14)$$

$$H = \sum_{i=1}^k \frac{(T_i - \mu_{T_i})^2}{\sigma_{T_i}^2} = \frac{12}{N(N+1)} \sum \frac{T_i^2}{n_i} - 3(N+1) \quad (15)$$

where μ_{T_i} = expectation of rank sum T_i in group i ; σ_{T_i} = variance of rank sum T_i in group i ; H = test statistic. Here H is set to follow the message: “Distribution is the same in the different configurations” [18]. After H is calculated, the p -value can be determined by a look-up table. According to this method the above data including vehicle speed, fuel cell power, battery power and electric motor torque are processed.

4.2. Non-Parametric Test of Vehicle Speed

Assuming that “vehicle speed distribution is the same in the different configurations”, if p -value is greater than 0.05, the hypothesis is established.

The box charts in Figure 14a,b show vehicle speed expressed in two categories to analyze the median, quartile, and tentacles lines of the different configurations and to calculate p -value. In Figure 14, the median, quartile, and tentacles lines of the different configurations are approximately same. In Configurations A1–A4 the one-way ANOVA method is used and $p = 1.000 > 0.050$. In Configurations B1–B3, $p = 0.008 < 0.050$.

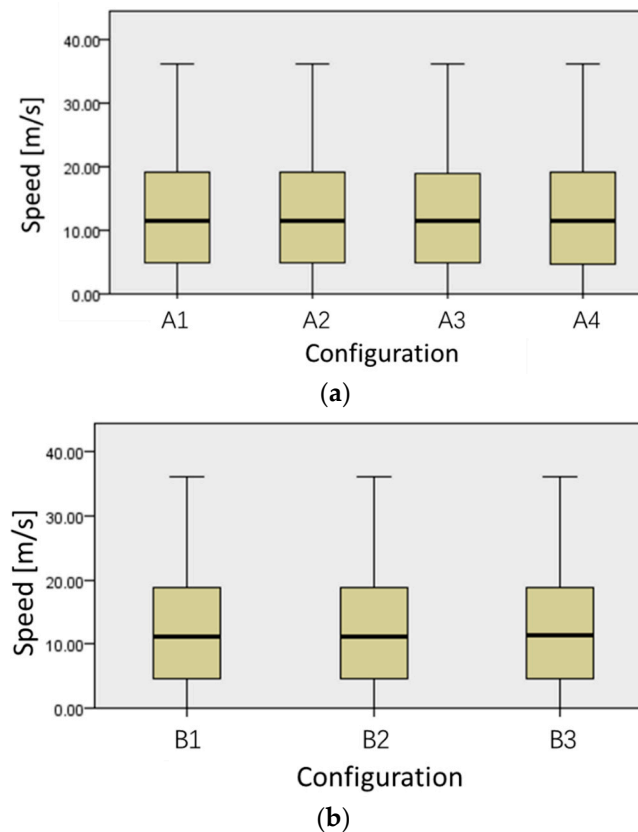


Figure 14. Box charts of vehicle speed under (a) Configurations A1–A4 and (b) Configurations B1–B3.

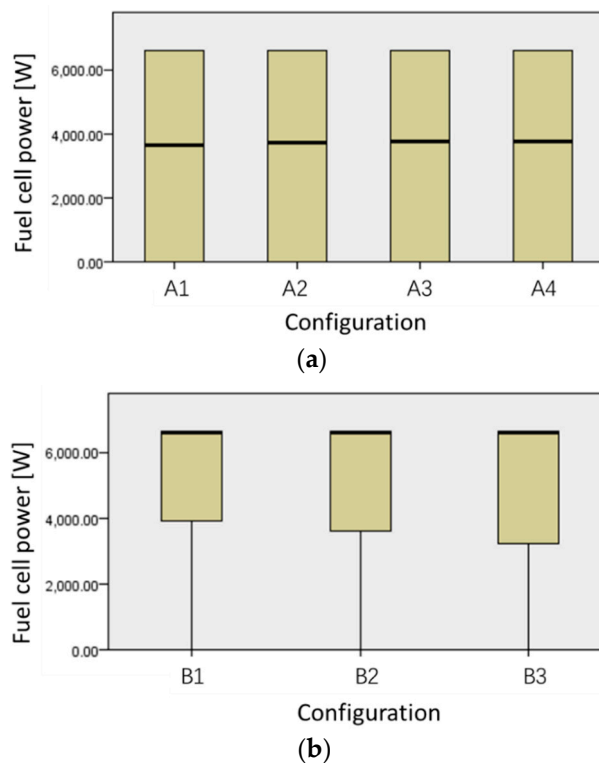
Table 18 shows the comparison of two configurations. As can be seen from Figure 14 and Table 18, the two significant differences between the two configurations of Configurations A1–A4 are greater than 0.05, as well as the two significant differences between Configurations B1–B3 are less than 0.05; thus, no significant difference exists in the transparency of Configurations A1–A4 for the variable of the vehicle speed, but the transparency of Configurations B1–B3 is significantly different.

Table 18. Comparison of two configurations under different configurations.

Sample1-Sample2	Test Statistic	Std. Test Statistic	Sig.	Adj. Sig.
Configuration A1–A3	529.265	0.611	0.541	1.000
Configuration A3–A4	−667.577	−0.771	0.441	1.000
Configuration A2–A3	743.746	0.859	0.390	1.000
Configuration A1–A4	−138.311	−0.160	0.873	1.000
Configuration A1–A2	−214.480	−0.248	0.804	1.000
Configuration A2–A4	76.169	0.088	0.930	1.000
Configuration B1–B2	1450.539	2.794	0.005	0.016
Configuration B1–B3	1312.237	2.528	0.011	0.034
Configuration B2–B3	−138.302	−0.266	0.790	1.000

4.3. Nonparametric Test of Fuel Cell Power

Assuming that “fuel cell power distribution is the same in the different configurations”, if the p -value is greater than 0.05, the hypothesis is approved. The box charts in Figure 15a,b show fuel cell power expressed in two categories to analyze the median, quartile, and tentacles lines of the different configurations and to calculate the p -value.

**Figure 15.** Box charts of fuel cell power under (a) Configurations A1–A4 and (b) Configurations B1–B3.

In Configurations A1–A4 and Configurations B1–B3, $p = 0.000 < 0.050$, which rejects the assumption that “fuel cell power distribution is the same in the structural category”.

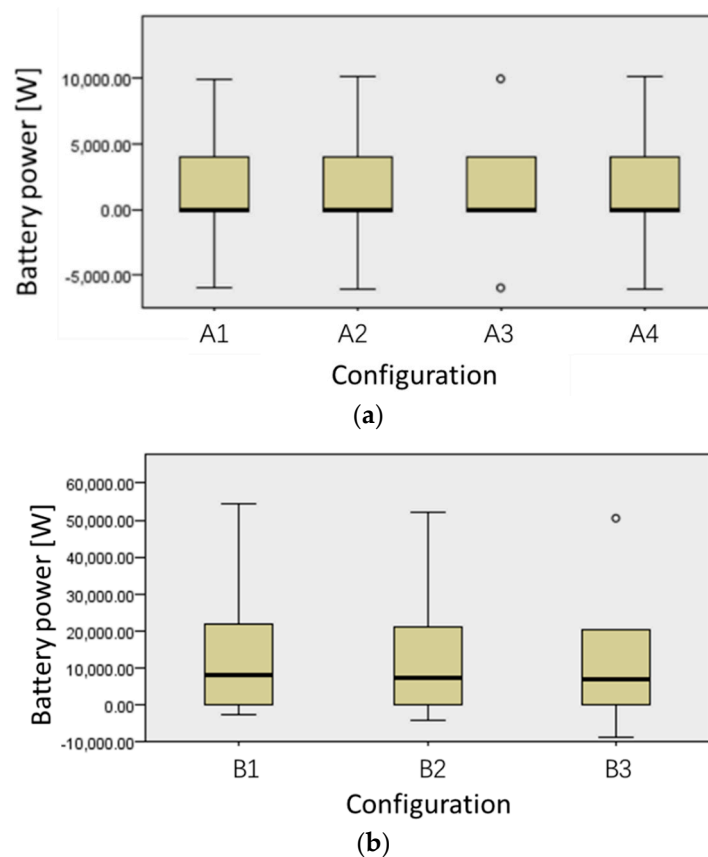
Table 19 compares several combinations of two configurations. As can be seen from Figure 15 and Table 19, only the significance between Configuration A1 and Configuration A3 and between Configuration A2 and Configuration A4 are greater than 0.05, and the other paired comparisons are less than 0.05.

Table 19. Comparison of two parameters under different configurations.

Sample1-Sample2	Test Statistics	Std. Test Statistic	Sig.	Adj. Sig.
Configuration A1–A3	−1478.020	−2.206	0.027	0.164
Configuration A1–A2	−3761.324	−5.615	0.000	0.000
Configuration A1–A4	−3976.797	−5.936	0.000	0.000
Configuration A2–A3	2283.304	3.408	0.001	0.004
Configuration A3–A4	−2498.778	−3.730	0.000	0.001
Configuration A2–A4	−215.473	−0.322	0.748	1.000
Configuration B1–B2	5665.610	12.855	0.000	0.000
Configuration B1–B3	8675.123	19.683	0.000	0.000
Configuration B2–B3	3009.513	6.828	0.000	0.000

4.4. Non-Parametric Test of Battery Power

Assuming that the “battery power distribution is the same in the different configurations”, if the p -value is greater than 0.05, the hypothesis is approved. Battery power is expressed in two categories, as can be seen from the box charts in Figure 16a,b, to analyze the median, quartile, and tentacles lines of the different configurations and to calculate p -value.

**Figure 16.** Box charts of vehicle speeds under (a) Configuration A1–A4 and (b) Configuration B1–B3.

For Configuration A1–A4 and B1–B3, $p = 0.000 < 0.050$, thus rejecting the assumption that “battery power distribution is the same in the structural category”.

Table 20 compares several different combinations of two configurations. As can be seen from Figure 16 and Table 20, only the significance between Configuration A2 and A3 is greater than 0.05, and the other paired configurations’ significance is less than 0.05.

Table 20. Comparisons of two parameters under different configurations.

Sample1-Sample2	Test Statistics	Std. Test Statistic	Sig.	Adj. Sig.
Configuration A1–A3	−2555.392	−3.804	0.000	0.001
Configuration A1–A2	−3137.662	−4.671	0.000	0.000
Configuration A1–A4	−6808.588	−10.136	0.000	0.000
Configuration A2–A3	582.270	0.867	0.386	1.000
Configuration A3–A4	−4253.197	−6.332	0.000	0.000
Configuration A2–A4	−3670.927	−5.465	0.000	0.000
Configuration B1–B2	5470.632	10.681	0.000	0.000
Configuration B1–B3	8268.968	16.145	0.000	0.000
Configuration B2–B3	2798.335	5.464	0.000	0.000

4.5. Non-Parametric Test of Electric Motor Torque

Assuming that the “electric motor torque distribution is the same in the different configurations”, if the p -value is greater than 0.05, the hypothesis is approved. Electric motor torque is expressed in two categories, as can be seen from the box charts in Figure 15a,b, to analyze the median, quartile, and tentacle lines of the different configurations and calculate p -value.

In Configurations A1–A4 and B1–B3, $p = 0.000 < 0.050$, which rejects the assumption that “electric motor torque distribution is the same in the structural category”.

Table 21 compares several configuration pairs. As can be seen from Figure 17 and Table 21, only the significance between paired combinations of Configurations A2, A3 and A4 are greater than 0.05, and the other paired configurations have a significance of less than 0.05.

Table 21. Comparison of two parameters under different configurations.

Sample1-Sample2	Test Statistics	Std. Test Statistic	Sig.	Adj. Sig.
Configuration A1–A3	−3822.682	−4.414	0.000	0.000
Configuration A1–A2	−4214.088	−4.866	0.000	0.000
Configuration A1–A4	−5229.778	−6.039	0.000	0.000
Configuration A2–A3	391.406	0.452	0.651	1.000
Configuration A3–A4	−1407.096	−1.625	0.104	1.000
Configuration A2–A4	−1015.690	−1.173	0.241	1.000
Configuration B1–B2	15285.072	29.436	0.000	0.000
Configuration B1–B3	24847.990	47.852	0.000	0.000
Configuration B2–B3	9562.919	18.416	0.000	0.000

4.6. Summary

From the above analysis it is clear that compared to hardware and software platforms, the transparency of simulated environments is higher and less affected by the network state. The speed and force output is relatively high compared to the power and energy output, which is less affected by the network. This summary is shown in Figure 18.

It is worth noting that the differences between transparency of speed, power, and torque are decided by the step of model building. This powertrain model contains a driver model, which keeps the desired speed and actual speed consistent. However, there are coupling relations between fuel cell power and battery power, and between electric motor torque and power source. Without decoupling the relations, the transparency of power and torque cannot directly measure the operator’s subjective responses to distributed remote test platforms.

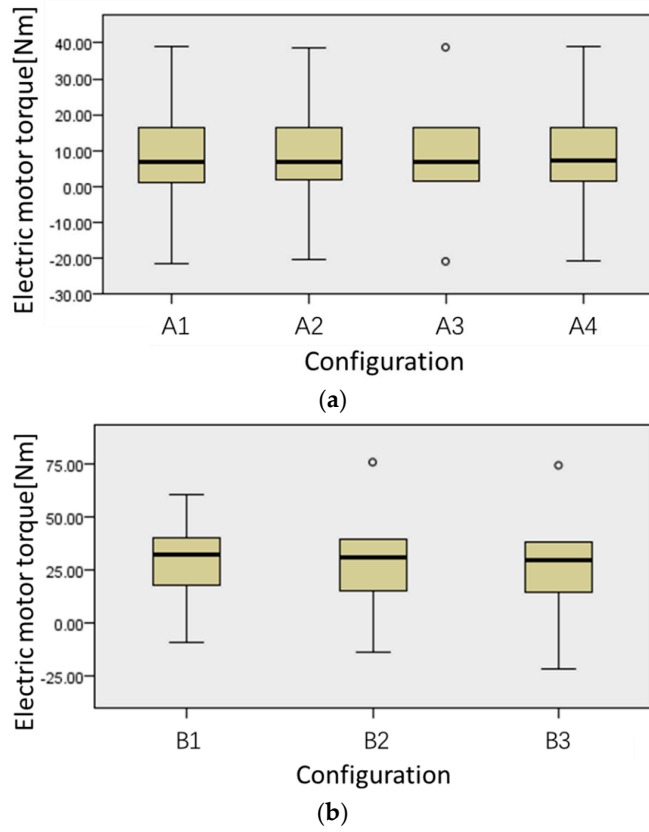


Figure 17. Box charts of electric motor torque under (a) Configurations A1–A4 and (b) Configuration B1–B3.

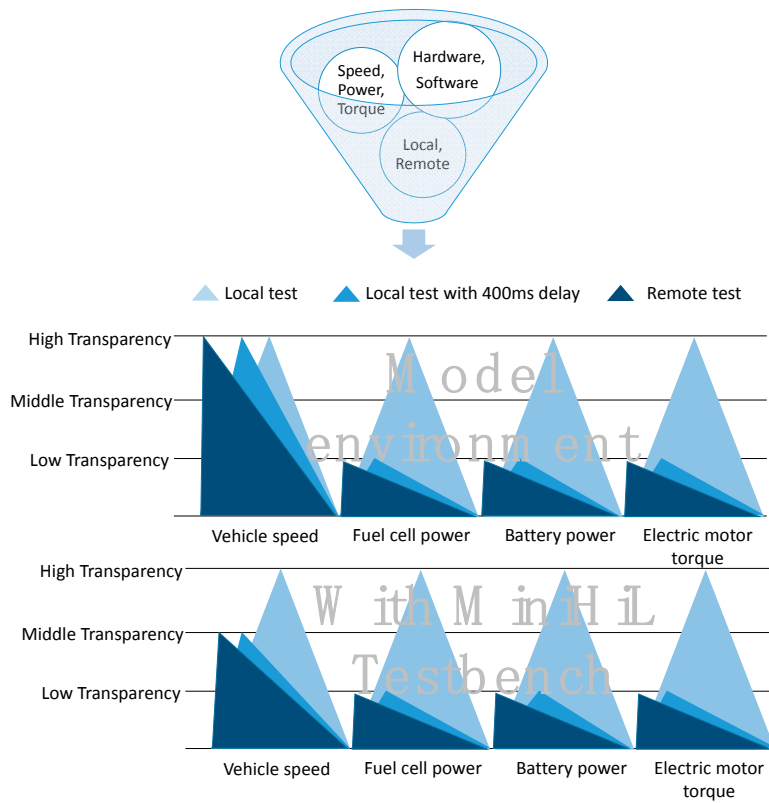


Figure 18. Summary of transparency types (high, middle, and low) under different configurations.

5. Conclusions

Based on the X-in-the-loop approach, a distributed test platform for a fuel cell automotive powertrain system was carried out, and the delay conditions under several different configurations are discussed. Combined with remote operating system and psychological knowledge, transparency measures the subjective feelings of remote distributed system operators with the values of several different configurations. The statistical significances of vehicle speed, fuel cell power, battery power, and electric motor torque are given under several configurations. With these statistical values the transparency of different configurations could be compared.

- (1) Models of fuel cell automotive powertrain system are developed and several tests of different configurations are carried out based on this system. The results show that vehicle speed, electric motor torque, battery power, and fuel cell power are affected by network state, the degree of influence is enhanced in turn.
- (2) A nonparametric detection method is used to analyze the impact of configuration settings, that is, transparency. Network state and operating environment on different observed signals jointly affect transparency. This result helps developer to adjust the configuration settings according to target signal in the test.

As future work, the authors would like to study the following issues: (a) decoupling the relations of power and torque; (b) facilitating the development of relevant remote tests and the discussion of test standards; and (c) exploring improvement of transparency using the XiL testing method.

Author Contributions: All authors planned the study; W.N. and Q.X. was involved in conceiving the methodology and performed the experiments; W.N. analyzed the data and wrote the paper; A.A., T.Z. and M.B. contributed the XiL concept and its application; K.S. contributed to the integrity of the work as a whole; and, finally, all authors have been involved in the analysis of the results and the obtaining of the conclusions.

Funding: This work was supported by the Chinese Ministry of Science and Technology under the project “Sino-German Fuel Cell Vehicle International Cooperation (Demonstration and Application)”, project number 2017YFB0103101, and Chinese National key R & D program “Reference Implementation and Verification Platform of Reconfigurable Intelligent Production System”, project number 2017YFE0101400. This work was also supported by the German Federal Ministry of Education and Research under the project “Methods for distributed spatially distributed development of H2 fuel cell vehicles in cooperation with China (MorEH2)”, project number 16EMO0316.

Conflicts of Interest: The authors declare no conflict of interest.

Abbreviations

ANOVA	Analysis of Variance
XiL	X-in-the-loop
MiniHiL	Mini Hardware in loop test bench
ECU	Electric Control Unit
PEMFC	Proton Exchange Membrane Fuel Cell
SOC	State of Charge
CC	Constant Charging
OCV	Open Circuit Voltage
UDP	User Datagram Protocol
VPN	Virtual Private Network
CAN	Controller Area Network
WLTC	Worldwide harmonized Light Duty Test Cycle

References

1. Tang, D.; Eversheim, W.; Schuh, G. A New Generation of Cooperative Development Paradigm in the Tool and Die Making Branch: Strategy and Technology. *Robot. Comput.-Integr. Manuf.* **2004**, *20*, 301–311. [[CrossRef](#)]
2. Gassmann, O.; Zedtwitz, M. New Concepts and Trends in International R&D Organization. *Res. Policy* **1999**, *28*, 231–250.

3. Albers, A.; You, Y.; Klingler, S.; Behrendt, M.; Zhang, T.; Song, K. A New Validation Concept for Globally Distributed Multidisciplinary Product Development. In Proceedings of the 20th International Conference on Industrial Engineering and Engineering Management, Baotou, China, 16–19 August 2013; Springer: Berlin/Heidelberg, Germany, 2013; pp. 231–242.
4. Albers, A.; Düser, T. Implementation of a Vehicle-in-the-Loop Development and Validation Platform. In Proceedings of the FISITA World Automotive Congress, Budapest, Hungary, 30 May–4 June 2010; F2010-C-177. FISITA: Stansted, UK, 2010.
5. Albers, A.; Behrendt, M.; Klingler, S.; Matros, K. Verifikation und Validierung im Produktentstehungsprozess. In *Handbuch Produktentwicklung*; Lindemann, U., Ed.; Carl Hanser Verlag: München, Germany, 2016; pp. 541–569.
6. Lundstrom, B.; Palmintier, B.; Rowe, D.; Ward, J.; Moore, T. Trans-oceanic remote power hardware-in-the-loop: Multi-site hardware, integrated controller, and electric network co-simulation. *IET Gener. Transm. Distrib.* **2017**, *11*, 4688–4701. [[CrossRef](#)]
7. Mayet, C.; Delarue, P.; Bouscayrol, A.; Chattot, E. Hardware-in-the-loop simulation of traction power supply for power flows analysis of multitrain subway lines. *IEEE Trans. Veh. Technol.* **2017**, *66*, 5564–5571. [[CrossRef](#)]
8. Liu, H.; Zhang, Y.; Yang, T. Blockchain-Enabled Security in Electric Vehicles Cloud and Edge Computing. *IEEE Netw.* **2018**, *32*, 78–83. [[CrossRef](#)]
9. Zhang, Y.; Lu, S.; Yang, Y.; Guo, Q. Internet-distributed vehicle-in-the-loop simulation for HEVs. *IEEE Trans. Veh. Technol.* **2018**, *67*, 3729–3739. [[CrossRef](#)]
10. Uhlemann, E. Connected-Vehicles Applications Are Emerging [Connected Vehicles]. *IEEE Veh. Technol. Mag.* **2016**, *11*, 25–96. [[CrossRef](#)]
11. Contu, S.; Marini, F.; Cappello, L.; Masia, L. Robot-assisted Assessment of Wrist Proprioception: Does Wrist Proprioceptive Acuity Follow Weber’s Law? In Proceedings of the 38th Annual International Conference of the IEEE Engineering in Medicine and Biology Society (EMBC), Orlando, FL, USA, 16–20 August 2016; IEEE: New York, NY, USA, 2016.
12. Naerum, E.; Hannaford, B. Global transparency analysis of the Lawrence teleoperator architecture. In Proceedings of the IEEE International Conference on Robotics and Automation, Kobe, Japan, 12–17 May 2009; IEEE: New York, NY, USA, 2009; pp. 3866–3871.
13. Lawrence, D.A. Stability and Transparency in Bilateral Teleoperation. *IEEE Trans. Robot. Autom.* **1993**, *9*, 624–637. [[CrossRef](#)]
14. Çavusoglu, M.C.; Sherman, A.; Tendick, F. Design of Bilateral Teleoperation Controllers for Haptic Exploration and Telemanipulation of Soft Environments. *IEEE Trans. Robot. Autom.* **2002**, *18*, 641–647. [[CrossRef](#)]
15. Natori, K.; Kubo, R.; Ohnishi, K. Transparency of Time Delayed Bilateral Teleoperation Systems with Communication Disturbance Observer. In Proceedings of the IEEE International Conference on Mechatronics, Changchun, Jilin, China, 8–10 May 2007; IEEE: New York, NY, USA, 2007.
16. Takagi, T. Traffic Flow Optimization by Weber-Fechner Law Applied Intelligent Vehicles. *J. Instrum. Autom. Syst.* **2014**, *1*, 50–55. [[CrossRef](#)]
17. Sakr, N.; Georganas, N.D.; Zhao, J. Human Perception-Based Data Reduction for Haptic Communication in Six-DoF Telepresence Systems. *IEEE Trans. Instrum. Meas.* **2011**, *60*, 3534–3546. [[CrossRef](#)]
18. Ersal, T.; Brudnak, M.; Stein, J.L.; Fathy, H.K. Statistical Transparency Analysis in Internet-distributed Hardware-in-the-loop Simulation. *IEEE/ASME Trans. Mechatron.* **2012**, *17*, 228–238. [[CrossRef](#)]
19. Yang, Y.; Peng, W.; Liu, J.; Wang, L. Analysis of Time-Varying Characteristics of Internet End-to-End Network Delay. *Commun. Comput. Inf. Sci.* **2012**, *345*, 436–445.
20. Yan, L.; Shen, H.; Chen, K. MobiT: Distributed and Congestion-Resilient Trajectory-Based Routing for Vehicular Delay Tolerant Networks. *IEEE/ACM Trans. Netw.* **2018**, *26*, 1078–1091. [[CrossRef](#)]
21. Gao, H.; Zhang, T.; Chen, H.; Zhao, Z.; Song, K. Application of the X-in-the-Loop Testing Method in the FCV Hybrid Degree Test. *Energies* **2018**, *11*, 433. [[CrossRef](#)]
22. Jazar, R.N. Vehicle dynamics: Theory and application. *J. Guid. Control Dyn.* **2014**, *33*, 287–288.
23. Song, K.; Li, F.; Hu, X.; He, L.; Niu, W.; Lu, S.; Zhang, T. Multi-mode energy management strategy for fuel cell electric vehicles based on driving pattern identification using learning vector quantization neural network algorithm. *J. Power Sources* **2018**, *389*, 230–239. [[CrossRef](#)]

24. Xu, L.; Xiao, J. Modeling and Simulation of the Dynamic Behavior of Proton Exchange Membrane Fuel Cell. *J. WUT (Inf. Manag. Eng.)* **2007**, *29*, 10–13. [[CrossRef](#)]
25. Xu, L.; Xiao, J. Modeling and simulation of PEM fuel cells based on electrochemical model. In Proceedings of the International Conference on Remote Sensing, Environment and Transportation Engineering, Nanjing, China, 24–26 June 2011; IEEE: New York, NY, USA, 2011.
26. Corrêa, J.M.; Farret, F.; Canha, L.N.; Simões, M.G. An electrochemical-based fuel-cell model suitable for electrical engineering automation approach. *IEEE Trans. Ind. Electron.* **2004**, *51*, 1103–1112. [[CrossRef](#)]
27. Khaligh, A.; Li, Z. Battery, ultracapacitor, fuel cell, and hybrid energy storage systems for electric, hybrid electric, fuel cell, and plug-in hybrid electric vehicles: State of the art. *IEEE Trans. Veh. Technol.* **2010**, *59*, 2806–2814. [[CrossRef](#)]
28. Zhou, D.; Al-Durra, A.; Matraji, I.; Ravey, A.; Gao, F. Online energy management strategy of fuel cell hybrid electric vehicles? A fractional-order extremum seeking method. *IEEE Trans. Ind. Electron.* **2018**, *65*, 6787–6799. [[CrossRef](#)]
29. Giordano, G.; Klass, V.; Behm, M.; Lindbergh, G.; Sjöberg, J. Model-based lithium-ion battery resistance estimation from electric vehicle operating data. *IEEE Trans. Veh. Technol.* **2018**, *67*, 3720–3728. [[CrossRef](#)]
30. Mini-Hardware-in-the-Loop Prüfstand als Entwicklungs- und Validierungsplattform. Available online: http://www.ipek.kit.edu/downloads/Mini-HiL_Flyer_141103.pdf (accessed on 6 November 2014).



© 2018 by the authors. Licensee MDPI, Basel, Switzerland. This article is an open access article distributed under the terms and conditions of the Creative Commons Attribution (CC BY) license (<http://creativecommons.org/licenses/by/4.0/>).